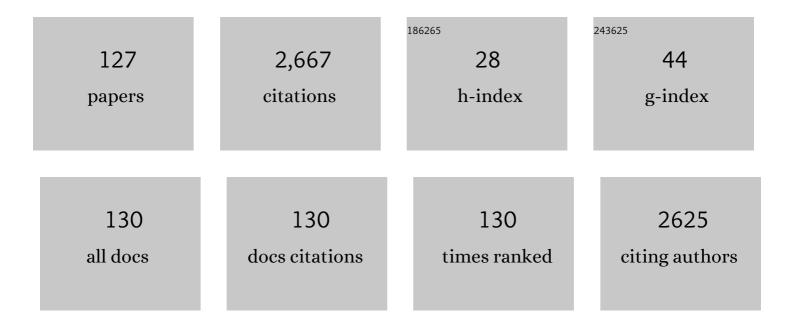
List of Publications by Year in descending order

Source: https://exaly.com/author-pdf/5770454/publications.pdf Version: 2024-02-01



#	Article	IF	CITATIONS
1	"APEC Blue†Secondary Aerosol Reductions from Emission Controls in Beijing. Scientific Reports, 2016, 6, 20668.	3.3	155
2	Observations of the vertical distributions of summertime atmospheric pollutants and the corresponding ozone productionÂinÂShanghai,ÂChina. Atmospheric Chemistry and Physics, 2017, 17, 14275-14289.	4.9	122
3	Satellite UV-Vis spectroscopy: implications for air quality trends and their driving forces in China during 2005–2017. Light: Science and Applications, 2019, 8, 100.	16.6	105
4	Haze insights and mitigation in China: An overview. Journal of Environmental Sciences, 2014, 26, 2-12.	6.1	91
5	Atmosphere boundary layer height and its effect on air pollutants in Beijing during winter heavy pollution. Atmospheric Research, 2019, 215, 305-316.	4.1	79
6	First observation of tropospheric nitrogen dioxide from the Environmental Trace Gases Monitoring Instrument onboard the GaoFen-5 satellite. Light: Science and Applications, 2020, 9, 66.	16.6	76
7	Transcriptomic Analyses of the Biological Effects of Airborne PM2.5 Exposure on Human Bronchial Epithelial Cells. PLoS ONE, 2015, 10, e0138267.	2.5	72
8	Characterization of ozone in the lower troposphere during the 2016 G20 conference in Hangzhou. Scientific Reports, 2017, 7, 17368.	3.3	67
9	Primary and secondary sources of ambient formaldehyde in the Yangtze River Delta based on Ozone Mapping and Profiler Suite (OMPS) observations. Atmospheric Chemistry and Physics, 2019, 19, 6717-6736.	4.9	60
10	Identification of long-range transport pathways and potential sources of PM2.5 and PM10 in Beijing from 2014 to 2015. Journal of Environmental Sciences, 2017, 56, 214-229.	6.1	56
11	Tropospheric NO ₂ , SO ₂ , and HCHO over the East China Sea, using ship-based MAX-DOAS observations and comparison with OMI and OMPS satellite data. Atmospheric Chemistry and Physics, 2018, 18, 15387-15402.	4.9	49
12	Label-free surface-sensitive photonic microscopy with high spatial resolution using azimuthal rotation illumination. Science Advances, 2019, 5, eaav5335.	10.3	48
13	Speciated atmospheric mercury on haze and non-haze days in an inland city in China. Atmospheric Chemistry and Physics, 2016, 16, 13807-13821.	4.9	45
14	Evolution of the vertical structure of air pollutants during winter heavy pollution episodes: The role of regional transport and potential sources. Atmospheric Research, 2019, 228, 206-222.	4.1	45
15	Identifying the wintertime sources of volatile organic compounds (VOCs) from MAX-DOAS measured formaldehyde and glyoxal in Chongqing, southwest China. Science of the Total Environment, 2020, 715, 136258.	8.0	45
16	Investigating the performance of a greenhouse gas observatory in Hefei, China. Atmospheric Measurement Techniques, 2017, 10, 2627-2643.	3.1	44
17	Ozone seasonal evolution and photochemical production regime in the polluted troposphere in eastern China derived from high-resolution Fourier transform spectrometry (FTS) observations. Atmospheric Chemistry and Physics, 2018, 18, 14569-14583.	4.9	42
18	Characteristics of aerosol size distribution and vertical backscattering coefficient profile during 2014 APEC in Beijing. Atmospheric Environment, 2017, 148, 30-41.	4.1	40

#	Article	IF	CITATIONS
19	Observations of ozone vertical profiles and corresponding precursors in the low troposphere in Beijing, China. Atmospheric Research, 2018, 213, 224-235.	4.1	40
20	High-resolution vertical distribution and sources of HONO and NO ₂ in the nocturnal boundary layer in urban Beijing, China. Atmospheric Chemistry and Physics, 2020, 20, 5071-5092.	4.9	40
21	Ship-based MAX-DOAS measurements of tropospheric NO ₂ , SO ₂ , and HCHO distribution along the Yangtze River. Atmospheric Chemistry and Physics, 2018, 18, 5931-5951.	4.9	38
22	Optimal chlorophyll fluorescence parameter selection for rapid and sensitive detection of lead toxicity to marine microalgae Nitzschia closterium based on chlorophyll fluorescence technology. Journal of Photochemistry and Photobiology B: Biology, 2019, 197, 111551.	3.8	38
23	Full-circle range and microradian resolution angle measurement using the orthogonal mirror self-mixing interferometry. Optics Express, 2018, 26, 10371.	3.4	37
24	Ozone profile retrievals from TROPOMI: Implication for the variation of tropospheric ozone during the outbreak of COVID-19 in China. Science of the Total Environment, 2021, 764, 142886.	8.0	34
25	An improved TROPOMI tropospheric HCHO retrieval over China. Atmospheric Measurement Techniques, 2020, 13, 6271-6292.	3.1	34
26	Characterization of temperature non-uniformity over a premixed CH4–air flame based on line-of-sight TDLAS. Applied Physics B: Lasers and Optics, 2016, 122, 1.	2.2	33
27	Investigations of temporal and spatial distribution of precursors SO ₂ and NO ₂ vertical columns in the North China Plain using mobile DOAS. Atmospheric Chemistry and Physics, 2018, 18, 1535-1554.	4.9	32
28	FTIR time series of stratospheric NO ₂ over Hefei, China, and comparisons with OMI and GEOS-Chem model data. Optics Express, 2019, 27, A1225.	3.4	32
29	Ground-based FTIR observation of hydrogen chloride (HCl) over Hefei, China, and comparisons with GEOS-Chem model data and other ground-based FTIR stations data. Optics Express, 2020, 28, 8041.	3.4	29
30	Haze observations by simultaneous lidar and WPS in Beijing before and during APEC, 2014. Science China Chemistry, 2015, 58, 1385-1392.	8.2	25
31	Preflight Evaluation of the Performance of the Chinese Environmental Trace Gas Monitoring Instrument (EMI) by Spectral Analyses of Nitrogen Dioxide. IEEE Transactions on Geoscience and Remote Sensing, 2018, 56, 3323-3332.	6.3	25
32	Development of a field system for measurement of tropospheric OH radical using laser-induced fluorescence technique. Optics Express, 2019, 27, A419.	3.4	25
33	Remote open-path cavity-ringdown spectroscopic sensing of trace gases in air, based on distributed passive sensors linked by km-long optical fibers. Optics Express, 2014, 22, 13170.	3.4	24
34	Development of a portable cavity ring down spectroscopy instrument for simultaneous, in situ measurement of NO3 and N2O5. Optics Express, 2018, 26, A433.	3.4	24
35	A dual dynamic chamber system based on IBBCEAS for measuring fluxes of nitrous acid in agricultural fields in the North China Plain. Atmospheric Environment, 2019, 196, 10-19.	4.1	24
36	Theoretical study of the red- and blue-shifted hydrogen bonds of nitroxyl and acetylene dimers. International Journal of Quantum Chemistry, 2006, 106, 2122-2128.	2.0	23

#	Article	IF	CITATIONS
37	A kinetic model for heterogeneous condensation of vapor on an insoluble spherical particle. Journal of Chemical Physics, 2014, 140, 024708.	3.0	23
38	A new method to determine the aerosol optical properties from multiple-wavelength O ₄ absorptions by MAX-DOAS observation. Atmospheric Measurement Techniques, 2019, 12, 3289-3302.	3.1	23
39	Real-Time Measurement of the Hygroscopic Growth Dynamics of Single Aerosol Nanoparticles with Bloch Surface Wave Microscopy. ACS Nano, 2020, 14, 9136-9144.	14.6	23
40	Determination of polycyclic aromatic hydrocarbons by four-way parallel factor analysis in presence of humic acid. Spectrochimica Acta - Part A: Molecular and Biomolecular Spectroscopy, 2016, 152, 384-390.	3.9	21
41	Diode laser cavity ring-down spectroscopy for in situ measurement of NO3 radical in ambient air. Journal of Quantitative Spectroscopy and Radiative Transfer, 2015, 166, 23-29.	2.3	20
42	Simultaneous measurement of NO and NO ₂ by a dual-channel cavity ring-down spectroscopy technique. Atmospheric Measurement Techniques, 2019, 12, 3223-3236.	3.1	20
43	Mapping the drivers of formaldehyde (HCHO) variability from 2015 to 2019 over eastern China: insights from Fourier transform infrared observation and GEOS-Chem model simulation. Atmospheric Chemistry and Physics, 2021, 21, 6365-6387.	4.9	20
44	The channel radius and energy of cloud-to-ground lightning discharge plasma with multiple return strokes. Physics of Plasmas, 2014, 21, 033503.	1.9	19
45	The design of rapid turbidity measurement system based on single photon detection techniques. Optics and Laser Technology, 2015, 73, 44-49.	4.6	19
46	Comparison of mixing layer height inversion algorithms using lidar and a pollution case study in Baoding, China. Journal of Environmental Sciences, 2019, 79, 81-90.	6.1	19
47	Self-Mixing Fiber Ring Laser Velocimeter With Orthogonal-Beam Incident System. IEEE Photonics Journal, 2014, 6, 1-11.	2.0	18
48	All-Fiber Configuration Laser Self-Mixing Doppler Velocimeter Based on Distributed Feedback Fiber Laser. Sensors, 2016, 16, 1179.	3.8	18
49	On-line analysis of algae in water by discrete three-dimensional fluorescence spectroscopy. Optics Express, 2018, 26, A251.	3.4	18
50	Vertical distributions of wintertime atmospheric nitrogenous compounds and the corresponding OH radicals production in Leshan, southwest China. Journal of Environmental Sciences, 2021, 105, 44-55.	6.1	18
51	A ultra-small-angle self-mixing sensor system with high detection resolution and wide measurement range. Optics and Laser Technology, 2017, 91, 92-97.	4.6	17
52	Fourier transform infrared time series of tropospheric HCN in eastern China: seasonality, interannual variability, and source attribution. Atmospheric Chemistry and Physics, 2020, 20, 5437-5456.	4.9	17
53	Mercaptopropionic acid-capped Mn-doped ZnS quantum dots as a probe for selective room-temperature phosphorescence detection of Pb ²⁺ in water. New Journal of Chemistry, 2017, 41, 13425-13434.	2.8	16
54	Estimation of winter time NOx emissions in Hefei, a typical inland city of China, using mobile MAX-DOAS observations. Atmospheric Environment, 2019, 200, 228-242.	4.1	16

#	Article	IF	CITATIONS
55	Vertical distributions of tropospheric SO2 based on MAX-DOAS observations: Investigating the impacts of regional transport at different heights in the boundary layer. Journal of Environmental Sciences, 2021, 103, 119-134.	6.1	16
56	Lidar vertical observation network and data assimilation reveal key processes driving the 3-D dynamic evolution of PM _{2.5} concentrations over the North China Plain. Atmospheric Chemistry and Physics, 2021, 21, 7023-7037.	4.9	16
57	Detection of heavy metals in water samples by laser-induced breakdown spectroscopy combined with annular groove graphite flakes. Plasma Science and Technology, 2019, 21, 034002.	1.5	15
58	Development of a laser heterodyne spectroradiometer for high-resolution measurements of CO ₂ , CH ₄ , H ₂ O and O ₂ in the atmospheric column. Optics Express, 2021, 29, 2003.	3.4	15
59	Using Lidar technology to assess regional air pollution and improve estimates of PM _{2.5} transport in the North China Plain. Environmental Research Letters, 2020, 15, 094071.	5.2	15
60	Intercomparison of NO x , SO2, O3, and aromatic hydrocarbons measured by a commercial DOAS system and traditional point monitoring techniques. Advances in Atmospheric Sciences, 2004, 21, 211-219.	4.3	14
61	Observations of New Particle Formation, Subsequent Growth and Shrinkage during Summertime in Beijing. Aerosol and Air Quality Research, 2016, 16, 1591-1602.	2.1	14
62	Phytoplankton photosynthetic rate measurement using tunable pulsed light induced fluorescence kinetics. Optics Express, 2018, 26, A293.	3.4	14
63	Elevated dust layers inhibit dissipation of heavy anthropogenic surface air pollution. Atmospheric Chemistry and Physics, 2020, 20, 14917-14932.	4.9	14
64	Number size distribution of atmospheric particles in a suburban Beijing in the summer and winter of 2015. Atmospheric Environment, 2018, 186, 32-44.	4.1	13
65	Real-world gaseous emission characteristics of natural gas heavy-duty sanitation trucks. Journal of Environmental Sciences, 2022, 115, 319-329.	6.1	13
66	Vertical profile of aerosol number size distribution during a haze pollution episode in Hefei, China. Science of the Total Environment, 2022, 814, 152693.	8.0	13
67	Scanning vertical distributions of typical aerosols along the Yangtze River using elastic lidar. Science of the Total Environment, 2018, 628-629, 631-641.	8.0	12
68	Retrieval of Global Carbon Dioxide From TanSat Satellite and Comprehensive Validation With TCCON Measurements and Satellite Observations. IEEE Transactions on Geoscience and Remote Sensing, 2022, 60, 1-16.	6.3	12
69	Ammonium nitrate is a risk for environment: A case study of Beirut (Lebanon) chemical explosion and the effects on environment. Ecotoxicology and Environmental Safety, 2021, 210, 111834.	6.0	12
70	Calibration-free wavelength modulation spectroscopy for gas concentration measurements using a quantum cascade laser. Applied Physics B: Lasers and Optics, 2017, 123, 1.	2.2	11
71	Emission Flux Measurement Error with a Mobile DOAS System and Application to NOx Flux Observations. Sensors, 2017, 17, 231.	3.8	11
72	Characterization of urban CO2 column abundance with a portable low resolution spectrometer (PLRS): Comparisons with GOSAT and GEOS-Chem model data. Science of the Total Environment, 2018, 612, 1593-1609.	8.0	11

#	Article	IF	CITATIONS
73	Long-distance mobile MAX-DOAS observations of NO2 and SO2 over the North China Plain and identification of regional transport and power plant emissions. Atmospheric Research, 2020, 245, 105037.	4.1	11
74	Vertical profile of aerosols in the Himalayas revealed by lidar: New insights into their seasonal/diurnal patterns, sources, and transport. Environmental Pollution, 2021, 285, 117686.	7.5	11
75	Design and Evaluation of an Aerosol Electrometer with Low Noise and a Wide Dynamic Range. Sensors, 2018, 18, 1614.	3.8	10
76	Validation of Water Vapor Vertical Distributions Retrieved from MAX-DOAS over Beijing, China. Remote Sensing, 2020, 12, 3193.	4.0	10
77	The Determination of Aerosol Distribution by a No-Blind-Zone Scanning Lidar. Remote Sensing, 2020, 12, 626.	4.0	10
78	<i>In Situ</i> Quantitative Observation of Hygroscopic Growth of Single Nanoparticle Aerosol by Surface Plasmon Resonance Microscopy. Analytical Chemistry, 2020, 92, 11062-11071.	6.5	10
79	Quantifying variability, source, and transport of CO in the urban areas over the Himalayas and Tibetan Plateau. Atmospheric Chemistry and Physics, 2021, 21, 9201-9222.	4.9	10
80	Aerosol Pollution Characterization before Chinese New Year in Zhengzhou in 2014. Aerosol and Air Quality Research, 2019, 19, 1294-1306.	2.1	10
81	Blind separation of fluorescence spectra using sparse nonâ€negative matrix factorization on right hand factor. Journal of Chemometrics, 2015, 29, 442-447.	1.3	9
82	On the Performance of an Aerosol Electrometer with Enhanced Detection Limit. Sensors, 2018, 18, 3889.	3.8	9
83	Characteristics and applications of near-infrared emissions from lightning. Journal of Applied Physics, 2013, 114, 163303.	2.5	8
84	The Influence of Instrumental Line Shape Degradation on the Partial Columns of O3, CO,CH4 and N2O Derived from High-Resolution FTIR spectrometry. Remote Sensing, 2018, 10, 2041.	4.0	8
85	Measurement of tropospheric HO2 radical using fluorescence assay by gas expansion with low interferences. Journal of Environmental Sciences, 2021, 99, 40-50.	6.1	8
86	A hydroxyl radical detection system using gas expansion and fast gating laser-induced fluorescence techniques. Journal of Environmental Sciences, 2018, 65, 190-200.	6.1	7
87	Design and evaluation of a unipolar aerosol particle charger with built-in electrostatic precipitator. Instrumentation Science and Technology, 2018, 46, 326-347.	1.8	7
88	Development of a static test apparatus for evaluating the performance of three PM2.5 separators commonly used in China. Journal of Environmental Sciences, 2020, 87, 238-249.	6.1	7
89	An automated dynamic chamber system for exchange flux measurement of reactive nitrogen oxides (HONO and NOX) in farmland ecosystems of the Huaihe River Basin, China. Science of the Total Environment, 2020, 745, 140867.	8.0	7
90	Reconstruction of a leaking gas cloud from a passive FTIR scanning remote-sensing imaging system. Applied Optics, 2021, 60, 9396.	1.8	7

#	Article	IF	CITATIONS
91	Nocturnal atmospheric chemistry of NO3 and N2O5 over Changzhou in the Yangtze River Delta in China. Journal of Environmental Sciences, 2022, 114, 376-390.	6.1	7
92	Measurement of HONO flux using the aerodynamic gradient method over an agricultural field in the Huaihe River Basin, China. Journal of Environmental Sciences, 2022, 114, 297-307.	6.1	7
93	Atmospheric Processing at the Seaâ€Land Interface Over the South China Sea: Secondary Aerosol Formation, Aerosol Acidity, and Role of Sea Salts. Journal of Geophysical Research D: Atmospheres, 2022, 127, .	3.3	7
94	Determination of Polycyclic Aromatic Hydrocarbons in the Presence of Humic Acid in water. Applied Spectroscopy, 2016, 70, 1520-1528.	2.2	6
95	Mercaptopropionic acid-capped Mn-doped ZnS quantum dots and Pb2+ as sensing system for rapid and sensitive room-temperature phosphorescence detection of sulfide in water. Journal of Photochemistry and Photobiology A: Chemistry, 2018, 364, 88-96.	3.9	6
96	Simulation of three-stage operating temperature for supersaturation water-based condensational growth tube. Journal of Environmental Sciences, 2020, 90, 275-285.	6.1	6
97	Study on Mash Gas Monitoring with Distributed Multipoint Fiber Optic Sensors System in Coal Mine. , 2012, , .		5
98	Remote sensing of chemical gas cloud emission by passive infrared scanning imaging system. , 2013, , .		5
99	Simulation of Miniature PDMA for Ultrafine-Particle Measurement. Atmosphere, 2019, 10, 116.	2.3	5
100	Concentration Quantification of Oil Samples by Three-Dimensional Concentration-Emission Matrix (CEM) Spectroscopy. Applied Sciences (Switzerland), 2020, 10, 315.	2.5	5
101	Development of a Laser Gas Analyzer for Fast CO2 and H2O Flux Measurements Utilizing Derivative Absorption Spectroscopy at a 100 Hz Data Rate. Sensors, 2021, 21, 3392.	3.8	5
102	Simultaneous detection of heavy metals in solutions by electrodeposition assisted laser induced breakdown spectroscopy. Journal of Laser Applications, 2022, 34, 012021.	1.7	5
103	Study on Physical Characteristics of a Bipolar Cloud-to-Ground Lightning Discharge Plasma. IEEE Transactions on Plasma Science, 2015, 43, 851-856.	1.3	4
104	Comparative study of cylindrical and parallelâ€plate electrophoretic separations for the removal of ions and subâ€⊋3Ânm particles. Journal of Separation Science, 2017, 40, 4813-4824.	2.5	4
105	Development and Application of HECORA Cloud Retrieval Algorithm Based On the O2-O2 477 nm Absorption Band. Remote Sensing, 2020, 12, 3039.	4.0	4
106	A Build-In Data Inversion Method to Retrieve Aerosol Size Distributions for a Portable Ultrafine Particle Sizer (PUPS). IEEE Access, 2021, 9, 2879-2889.	4.2	4
107	Research on information acquisition and manipulation representation (MR) method of traditional chinese medical massage (TCMM) based on multi-dimension force sensor. , 2015, , .		3
108	Using Lidar, in-situ measurements and Trajectory Analysis to observe air pollution in Beijing, 2014. EPJ Web of Conferences, 2016, 119, 24008.	0.3	3

#	Article	IF	CITATIONS
109	Feature issue introduction: light, energy and the environment, 2017. Optics Express, 2018, 26, A636.	3.4	3
110	Design and evaluation of a condensation particle counter with high performance for single-particle counting. Instrumentation Science and Technology, 2020, 48, 212-229.	1.8	3
111	Retrieval of refractive index of ultrafine single particle using hygroscopic growth factor obtained by high sensitive surface plasmon resonance microscopy. Journal of Environmental Sciences, 2023, 126, 483-493.	6.1	3
112	Three-dimensional reconstruction of a leaking gas cloud based on two scanning FTIR remote-sensing imaging systems. Optics Express, 2022, 30, 25581.	3.4	3
113	Correlation study between suspended particulate matter and DOAS data. Advances in Atmospheric Sciences, 2006, 23, 461-467.	4.3	2
114	Development of respirable virtual-cyclone samplers. Journal of Occupational and Environmental Hygiene, 2019, 16, 785-792.	1.0	2
115	Analysis and Adjustment of Positioning Error of PSD System for Mobile SOF-FTIR. Sensors, 2019, 19, 5081.	3.8	2
116	An active RH-controlled dry-ambient aerosol size spectrometer (DAASS) for the accurate measurement of ambient aerosol water content. Journal of Aerosol Science, 2021, 158, 105831.	3.8	2
117	Characterization of submicron aerosol particles in winter at Albany, New York. Journal of Environmental Sciences, 2022, 111, 118-129.	6.1	2
118	Technical note: Real-time diagnosis of the hygroscopic growth micro-dynamics of nanoparticles with Fourier transform infrared spectroscopy. Atmospheric Chemistry and Physics, 2022, 22, 3097-3109.	4.9	2
119	Impacts of imperfect geometry structure on the nonlinear and chromatic dispersion properties of a microstructure fiber. Applied Optics, 2007, 46, 7771.	2.1	1
120	Research and design of resonant mass sensor based on tapered oscillating element. Proceedings of SPIE, 2009, , .	0.8	1
121	Underdetermined blind separation of three-way fluorescence spectra of PAHs in water. Spectrochimica Acta - Part A: Molecular and Biomolecular Spectroscopy, 2018, 199, 80-85.	3.9	1
122	Heterogeneous reaction and condensation growth observation of NaCl/dicarboxylic acids nanoparticles by aerosol time-of-flight mass spectrometer with water-based particle size amplifier. Atmospheric Environment, 2021, 246, 118162.	4.1	1
123	Open-path Detection Of Atmospheric CH4 And N2O Based On Quantum Cascade Laser. , 2014, , .		1
124	Advances in coastal ocean boundary layer detection technology and equipment in China. Journal of Environmental Sciences, 2022, , .	6.1	1
125	Design of On-Line Measurement System for Fine Particle Number Concentration of Vehicle Exhaust Based on Diffusion Charge Theory. Lecture Notes in Electrical Engineering, 2019, , 1874-1884.	0.4	0
126	Concentration-Emission Matrix (CEM) Spectroscopy Combined with GA-SVM: An Analytical Method to Recognize Oil Species in Marine. Molecules, 2020, 25, 5124.	3.8	0

	Jiai	Jianguo Liu	
#	Article	IF	CITATIONS
127	Development and Application of a Wide Dynamic Range and High Resolution Atmospheric Aerosol Water-Based Supersaturation Condensation Growth Measurement System. Atmosphere, 2021, 12, 55	8. 2.3	Ο